SIMULATION AND ANALYSIS OF ELECTRIC MOTOR FAILURE DURING E-VTOL AIRCRAFT OPERATIONS IN TURBULENT AIRWAKE

Jan Goericke, jan.goericke@flightlab.com, Advanced Rotorcraft Technology, Inc., Fremont, CA, USA
Felix Brenner, f.brenner@gtisoft.com, Gamma Technologies, LLC Stuttgart, Germany
Dooyong Lee, PhD, dooyong.lee@flightlab.com, Advanced Rotorcraft Technology, Inc., Fremont, CA, USA

Abstract

eVTOL aircraft in advanced air mobility applications and in support of urban passenger transport are expected to operate from vertiports located on rooftops and other structures. This study illustrates a single design iteration for such an aircraft exercising comprehensive modeling and simulation coupled with a detailed, physics-based propulsion system model and with special consideration of operations in the turbulent urban airwake environment. It is investigated whether detailed aircraft simulation can identify crucial system requirements early in the design phase and ultimately help focus and accelerate the development process. The simulation tools are applied specifically to an approach and hover hold maneuver in an urban turbulent airwake in support of flight control and electric propulsion systems design. A single electric motor fault is explored to derive the requirements for the design and sizing of the electric propulsion system components and the flight controller. The study concludes with a list of items for the follow-on design iteration.

1. INTRODUCTION

Previous work has explored the feasibility of coupling a comprehensive VTOL modeling and simulation application with a physics-based electric propulsion model in a unified simulation approach, Refs. 1, 2, 3. It was found that setup times and data requirements for the coupled eVTOL simulation were manageable and made it feasible for use in conceptual aircraft design. The coupled simulation provided insight into system characteristics during flight maneuvers which could not be obtained by separate simulation execution. The benefits of coupled flight dynamics and detailed electric propulsion simulation were presented for turbulent operating environments in Ref. 1.

The aim of this paper is to exercise the coupled, physics-based simulation approach at an early stage of an eVTOL aircraft design iteration step. A business case is assumed to exist justifying the development and operation of a new aircraft system in for-profit applications. An aircraft design mission can be derived from the business case. Established and emerging VTOL modeling and simulation tools and techniques can support the early design stages and help derive aircraft and system-level requirements supporting competitive and accelerated time-to-service schedules. Furthermore, the early adoption of simulation directly supports a simulation-supported aircraft certification approach as currently explored by airworthiness authorities, the European Clean Sky 2 project Rotorcraft Certification by Simulation (Ref. 4), and the SAE G-35 working group.

This paper utilizes the models created in Ref.1 and applies the coupled simulation environment for an iteration of the conceptual design phase for a notional lift plus cruise eVTOL configuration. Figure 1 illustrates the aircraft design process followed in this paper with the focus on flight dynamics and electric propulsion modeling and simulation. A notional design mission is used for the initial sizing of the electric propulsion system. Comprehensive aircraft simulation and analysis will be used to generate initial predictions for the power required for the design mission. This information is used to size the main components of the electric propulsion system, design the thermal management systems, and energy storage requirements. The design mission includes operations from rooftop vertiports. The aircraft is therefore required to be capable of approaching, departing, and landing in a turbulent airwake environment. The coupled simulation of flight dynamics and detailed electric propulsion system is executed in the critical maneuvering flight operation of approach for landing in the turbulent urban air environment. The turbulent airwake environment is expected to stress the aircraft flight control and electric propulsion systems such that important design requirements may be derived in addition to the steady state required power estimates from the design mission. Additionally, a single lift rotor malfunction is executed for the purpose of informing the aircraft systems design. Consequently, following the process in Figure 1 will provide steady state and transient power requirements needed for sizing the electric propulsion system and designing the flight

Presented at 50th European Rotorcraft Forum, Marseille, France, 10-12 September 2024

controller. The detailed modeling and simulation of the electric propulsion system will provide initial component mass information needed for the refinement of the aircraft design in the next design iteration.

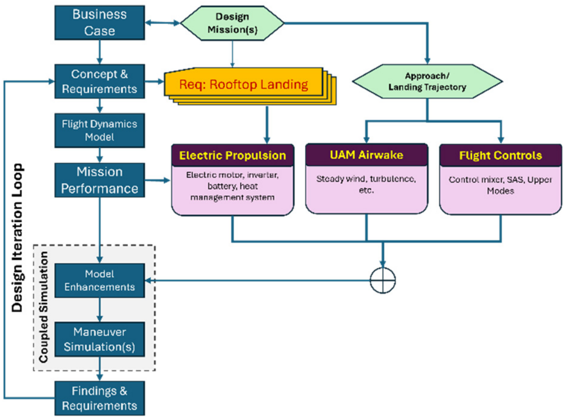

Figure 1: Illustration of Aircraft Design Iteration

The investigations conclude with the listing of next steps for follow-on aircraft design iterations. It shall be noted that this approach is applicable for investigating candidate eVTOL configurations for a given design mission. Since the process is expected to be similar for different aircraft configurations, it is not discussed in this study.

2. INITIAL AIRCRAFT DESIGN AND MODELS

The NASA lift plus cruise eVTOL conceptual design was used as an inspiration for the simulation model used in this study, Refs. 5, 6. Simulation is used to support early aircraft design in terms of top-level aircraft and system requirements, subsystem design and sizing, and aircraft subsystem weight estimates. It is assumed for this discussion that the lift plus cruise configuration was deemed most suitable for the mission in a prior configuration down selection. Note that naming in the following is consistent with the main purpose of aerodynamic systems such that *rotors* are used for lift and *propellers* for forward propulsion.

2.1. Lift Plus Cruise eVTOL Configuration

A rigid-body flight dynamics model (FDM) of a lift-plus-cruise eVTOL configuration based on Refs. 5, 6, and was generated using FLIGHTLAB, see Figure 2. The configuration consists of eight rigid-blade lift rotors mounted to fore and aft pylons off the wing box. The lift rotors were two-bladed, with a radius of 5 feet, and approximately 10 degrees of linear blade twist. The blade airfoil was approximated using aerodynamic coefficients as function of angles of attack and Mach number for the SC 1095 airfoil. An unsteady airloads model and 30 aerodynamic segments were used for the blade airloads. The rotor/propeller inflow and wake were modeled using the Peters-He finite state model. The three-bladed pusher propeller with a radius of approximately 4.5 ft was modeled similarly to the lift rotors. The lift rotor and pusher propeller models in this study were constant-speed, variable collective blade pitch-controlled for simplicity and to avoid the potentially significant time delays associated with variable speed control. The lift rotor and pusher propeller were operating at rotational speeds of 907 and 1,050 rpm, respectively. The rigid main wing with an approximately 48 ft wingspan featured a notional general aviation airfoil. The total vehicle weight was 5,800 lbs. The configuration included a fuselage airloads model with notional aerodynamic coefficients as a table look-up. The equivalent flat drag budget for the fuselage was set at 0.155 m^2 (1.67 ft^2). The vertical and horizontal tail surfaces were modeled as two-dimensional aerodynamic surfaces using aerodynamic coefficients of a symmetrical airfoil. Although a landing gear model was included in the simulation model, ground contact was not simulated in this investigation. An ideal engine model was implemented to support baseline simulations with the flight dynamics model with and without the turbulent airwake. It provided the rotor/propeller torque required to maintain the constant rotational speed without modeling the powertrain dynamics. The ideal engine model was also used during the development of the flight control system including control mixer, stability augmentation, and autopilot.

Figure 2: Example Lift Plus Cruise eVTOL Configuration from Refs. 5,6

The architecture of the flight control system used in this study is illustrated in Figure 3. It was implemented using the FLIGHTLAB Control System Graphical Editor and was as such part of the flight dynamics model in the coupled simulation. The flight control model consists of classical pilot stick controls, i.e., longitudinal, lateral, collective, and pedal, a stability augmentation system (SAS), and a hold modes controller which provides flight control inputs to follow a desired trajectory command. The flight control mixer for the lift plus cruise eVTOL configuration distributed the control inputs to the lift rotors and the pusher propeller. The study focused on equivalent airspeeds below 40 kts where fixed wing controls are largely ineffective. Aircraft pitch control was provided by differential thrust of the fore and aft lift rotors, lateral control by left/right differential thrust, and yaw control by a combination of differential torque and thrust of the canted lift propellers. A pusher propeller aft of the horizontal stabilizer provided forward thrust via a power level control input. Lift rotor and pusher propeller thrusts were controlled by variations of the blade collective pitch while maintaining a constant rotational speed.

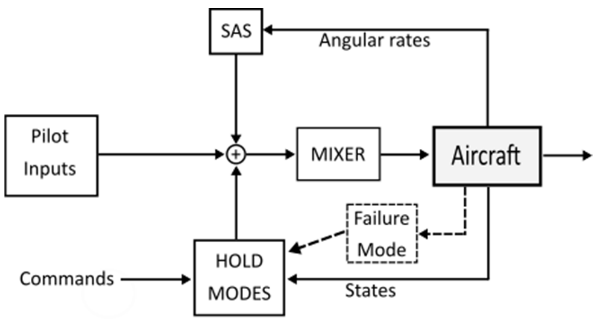

Figure 3: Schematic of Flight Control System for Lift Plus Cruise eVTOL Configuration

Stability augmentation systems play a crucial role in enhancing the stability and control of various vehicles, particularly rotorcraft. These systems utilize sensors to continuously monitor the vehicle's attitude and motion, adjusting to counteract disturbances and maintain desired flight characteristics. A SAS often employs advanced algorithms and actuators to provide rapid and precise corrections, ensuring that the vehicle remains stable under varying conditions such as turbulence or other external forces. By actively managing the aerodynamic surfaces or propulsion systems, stability augmentation systems contribute to overall safety and performance, allowing vehicles to navigate through challenging environments with increased reliability. In this study, feedback of the vehicle's angular rates, i.e., roll, pitch, and yaw, was used to enhance the stability of the aircraft.

The hold modes controller in Figure 3 had two major modes in the longitudinal and lateral channels, a velocity hold mode and a position hold mode. Both modes used "desired" velocity commands as inputs. While the velocity hold mode used the velocity command directly as the desired velocity, the position error was converted to desired velocities in the position hold mode. From the desired horizontal (x-y) velocity commands, the velocity error was calculated and passed through a PID controller for command following. The hold mode controller also provided the radar altitude hold mode via the collective channel and the heading hold mode using the yaw control channel. The SAS and hold modes controllers were developed and tuned for steady wind conditions using the ideal electric propulsion model. The flight controller was further tuned to allow for the simulation of a steady descent and hover hold over the landing spot in the urban airwake environment used in this paper.

The flight controller did not include fault mitigation algorithms (e.g. failure mode controller) consistent with the design maturity assumed for the discussion in this study. The fault was inserted for the target lift propeller and mirrored for the opposite lift propeller on the other side of the wing. The flight controller performed best effort of maintaining flight under fault conditions. The aircraft response was used to derive new requirements for the next iteration of flight control design. Further efforts are required to design a failure mode control algorithm which will adjust control parameters of the hold mode controller to detect and correct failures. These systems could use data driven methods to detect faults through input and output data, then reconfigure themselves to maintain the desired flight performance.

2.2. Design Mission

The "business case" was to provide an aerial and scheduled solution for transporting up to six people between the downtowns of San Francisco and San Jose with stops at two international airports (SFO and SJC) and the technology centers in Silicon Valley. The distance between San Francisco and San Jose is approximately 67 kilometers (42 miles) with driving times between 1 - 1.5 hours depending on traffic. The development of a real-world business case for urban air mobility was not the focus.

The simplistic design mission developed for the demonstration of the aircraft design process is illustrated in Figure 4. The mission consists of six segments for a flight from downtown San Francisco to San Jose in California. Each mission segment includes mission elements such as hover, vertical and forward climb, cruise flight, and descent. Flight levels did not consider controlled airspace requirements. Cruise flight was performed at approx. 1,000 - 1,500 ft above the ground. A 60 second hover started and ended each mission segment. Although variations of ambient conditions are important for aircraft design, this study focused on standard day atmospheric conditions since the same workflow is performed when exploring the flight and mission performance capabilities at non-standard atmospheric conditions such as elevated ambient temperatures. To conclude the “business case,” a similar mission profile is assumed to continue along the East Bay returning the aircraft to the original vertiport in San Francisco and with a stop at the Oakland International Airport (OAK).

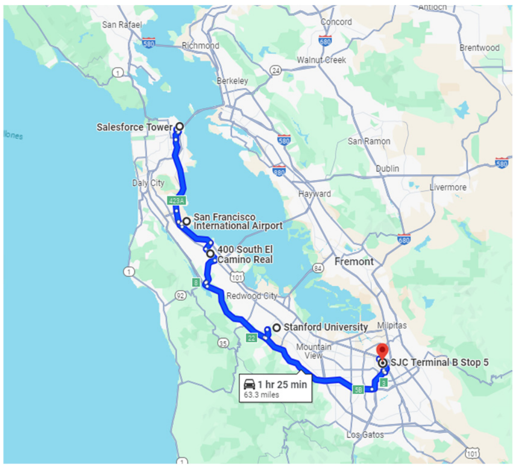

Figure 4: Example Design Mission

2.3. Design Mission Performance

The FLIGHTLAB mission calculator, see Figure 5, was used to assemble the design mission from a list of available mission elements. The mission calculator then executed the mission profile using the previously described lift plus cruise eVTOL simulation model. The design mission in Figure 4 shows the mission starts at a vertiport on the roof of a downtown building in San Francisco. After an initial departure check (hover), the aircraft climbs to cruise altitude before descending for approach to the next landing spot. The user specifies the initial flight and ambient conditions for each mission element (hover, climb, cruise, descent, etc.) in the mission calculator. The aircraft is trimmed, and flight performance parameters are collected before the next mission element is executed. After completion, the mission calculator integrates the flight duration, power required, and energy consumption for the entire mission. This process therefore provides the required steady state power for each mission element, the flight time, and the energy consumption. No drivetrain losses or component efficiencies were considered since the initial mission performance simulation in FLIGHTLAB was performed using an ideal engine propulsion model. The mission performance estimates were passed on to the electric propulsion group for sizing and design of the electric propulsion system including the predicted energy depletion for the entire design mission as estimated by the mission calculator. This information can be used to size the aircraft battery using consideration of the number of missions flown per battery charge.

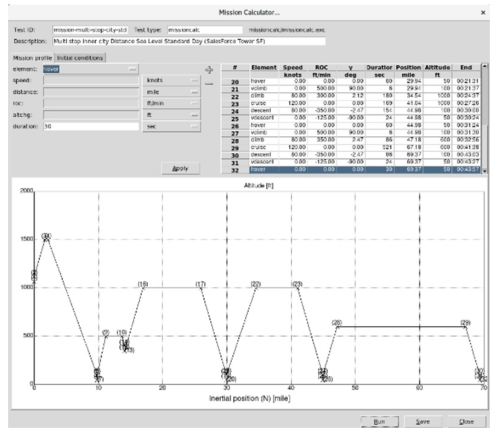

Figure 5: FLIGHTLAB Mission Calculator

Estimates for steady state required power for the lift rotor and pusher propeller are summarized for the mission elements in Table 1. Note that the trim solution was symmetric meaning that power of the wing leading edge lift rotors, #1 - #4, and trailing edge lift rotors, #5 - #8, were the same at a given mission element. Therefore, the table only shows the results for one of the rotors in the group.

Table 1: Power Required for Mission Elements

Mission Elements	**Power Required [kW]**		
	Rotors (L.E.)	**Rotors (T.E.)**	**Prop**
	#1 - 4	**#5 - 8**	**#9**
Hover	53.5	51.8	16.7
Vertical Climb (350 ft/min)	56.9	55.0	16.7
Vertical Climb (500 ft/min)	58.7	56.7	16.7
Forward Climb (80 kts, 200 ft/min)	0	0	75.6
Cruise (100 kts)	0	0	68.7
Cruise (120 kts)	0	0	101.7
Descent (80 kts, -200 ft/min)	0	0	18.2
Vertical descent (-125 ft/min)	52.5	50.0	16.7

2.4. Electric Propulsion Conceptual Design

The initial layout for the electric propulsion system is illustrated in Figure 6. The battery and its heat management system were placed in the wing/fuselage structures close to the desired aircraft center of gravity. Each rotor and propeller had dedicated models for an electric motor, inverter, and heat exchanger. The propulsion system from Ref. 1 was expanded with a detailed inverter model, new motor designs for lift rotors and pusher propeller, and a detailed thermal model of the motors.

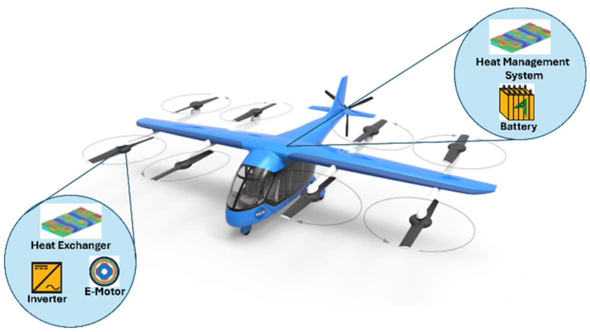

Figure 6: Schematic of Electric Propulsion System

The electric motors need to be designed to produce sufficient steady power for the design mission and transient power to support maneuvering flight requirements. The initial motor sizing and design used the mechanical requirements, e.g., speed, torque and power, obtained from the flight dynamics simulation in Table 1. As it is common in early aircraft design, a design margin of 20% was applied to account for transient power demands during maneuvering flight operations of the eVTOL in turbulent air environments and malfunction scenarios.

The Gamma Technologies GT-SUITE application was used for the design, modeling, and simulation of the electric propulsion system. The software application includes a tool for sizing electric motors to meet aircraft design requirements. The minimal set of design properties are motor output power, battery direct current (DC) voltage, and rated motor speed. Optional design properties including maximum current and information about the motor control algorithms can be supplied to increase the quality of the proposed motor design solutions.

Figure 7 shows a schematic of the applied electric powertrain design workflow. The initial motor design was obtained with the sizing tool using the required torques and speeds from the initial mission performance assessment and requirements for the electric motor voltage and current from prior subject matter experience. The inverter must convert the battery discharge power to alternating current (AC) power required by the electric motor. The battery needs to support the voltage and current draws from the inverter and store sufficient energy to support the design mission.

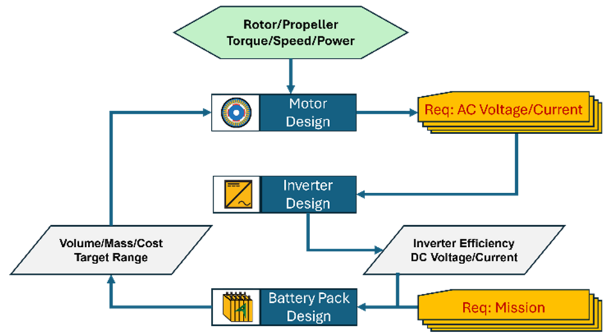

Figure 7: Powertrain Design Workflow

The inverters were designed to have an efficiency of 100% for the initial powertrain design. Modern power converters reach high efficiencies of 95-99% during ideal operating conditions. Therefore, accounting for a safety margin during detailed power converter design in later design stages justifies the applicability of an ideal inverter during early design stages. The battery pack must be sized to provide the necessary power even at low state of charge while keeping the inverter efficiency into account.

The initial powertrain design was evaluated by running a single unit of battery, power converter, and electric motor at the most demanding steady state operating conditions of the design mission. Next, the initial electric propulsion system was exercised in the coupled simulation with the flight dynamics model and within the turbulent airwake environment. Maneuvering flight simulations with the coupled models provided the transient effects, e.g., inertias of the drivetrain and interactions with the flight controls, which put additional demand on the electric powertrain components, and allowing to optimize not only single electric powertrain components one by one but the complete electric powertrain system concurrently.

Battery Initial Design

A preliminary model of the battery pack was created based on the initial motor design. An appropriately sized battery must provide sufficient power to run the electric motors at the given torque and speed requirements while providing enough capacity to maintain the power for the duration of the design mission and until recharging. Therefore, the key factors for early-stage battery design are battery chemistry and battery pack size. The battery design described in Ref 1 meets the power requirements to run the nine electric motors. Secondly, the capacity of the battery pack can be adjusted by increasing the number of parallel cells in the battery pack.

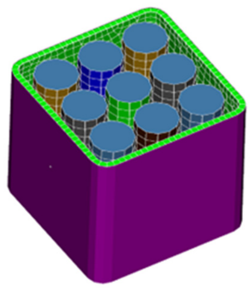

(a) Battery Pack and Housing

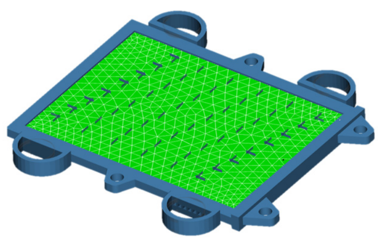

(b) Cooling Plate

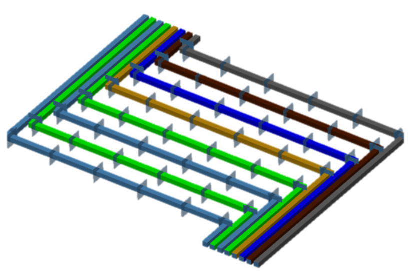

(c) Coolant Pipes

Figure 8: Illustration of Battery Pack and Cooling Circuit Components

The battery pack was designed using an electro-chemical battery simulation tool as described in Ref. 1. A Lithium-Nickel-Manganese-Cobalt-Oxide chemistry (NCM811) was used for the battery active material, along with a graphite cathode material. Cell chemistries of this type are known for providing high energy densities. The total pack weight with 7,600 individual cells was approximately 859 kg (1,894 lbm). The battery pack size was adjusted to be able to provide the voltage and power necessary to drive the nine motors of the eVTOL configuration and taking the inverter efficiency into account.

A thermal model of the battery was derived from the electro-chemical model of the pack. An illustration of such a 3D thermal battery model can be seen in Figure 8(a). The thermal model of the battery pack can be expanded by adding cooling components such as cooling plates and cooling channels to the 3D model. Cooling plates and cooling channels attached to the battery pack model from Ref 1. are illustrated in Figure 8(b) and Figure 8(c).

The thermal model of the battery pack itself as well as the thermal models of cooling plate and pipes were transformed and exported into a 1D thermal mass model. This allowed the thermal model of the battery pack to be integrated directly into the coupled system model containing the electrical powertrain and the flight dynamics model. With that, the heat loads calculated from the electrochemical battery model can be imposed on the thermal model directly to calculate the transient temperature distribution inside the battery pack. The battery temperature can then be fed back to the electrochemical model to account for the temperature dependencies of the electrochemical simulation.

2.5. Powertrain Design Refinement

After the initial component layout, the electric powertrain was evaluated in terms of battery capacity and the weight of the electric powertrain. The number of parallel battery cells was increased to increase the effective capacity of the battery pack and therefore increase the range of the eVTOL. This led to an increase in weight of the propulsion system. The electric motor design was revised to decrease the system weight. An electromagnetic analysis was performed in GT-SUITE to investigate the spread of the magnetic field lines inside the stator iron material. The results showed that a reduction of the stator iron thickness will not result in a significant loss of performance.

Exercising the coupled simulation allowed for a quick initial optimization of the performance and weight estimates of the components of the electric propulsion system. The powertrain can be further optimized using a single objective, e.g. optimizing the powertrain in terms of eVTOL range, or multiple objectives, e.g. additionally taking component/system weight into account.

Electric Motor Design Refinements

The electric motor was designed using the GT-SUITE 2D electromagnetic finite element analysis (FEA) tool described in Ref 1. The electric motors of the lift rotors were initially designed as radial flux interior permanent magnet (IPM) motors in Ref 1. This motor design was replaced with an axial flux motor (AFM) design. A schematic of the assembly for an axial flux machine is shown in Figure 9.

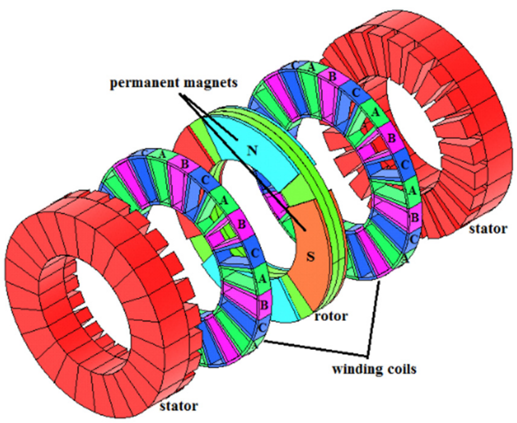

Figure 9: Schematic of Axial Flux Machine, Ref 7

While the axial flux motor also uses permanent magnets to interact with the rotating magnetic field induced by the stator winding, it can produce high torques while maintaining a compact design. AFMs are predominantly used in applications where component weight is a critical factor for system design. The electromagnetic simulation of axial flux machines is a 3D problem due to the geometry and direction of magnetic flux. The 3D machine geometry can, however, be approximated by linear motor geometry, see Figure 10, to use the less CPU intensive 2D FEA described in Ref 1. A so-called "2 Stator, 1 Rotor" configuration was chosen for the axial flux machine.

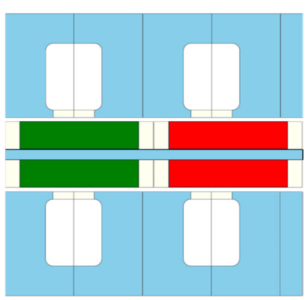

Figure 10: Section of 2D linear motor model

Figure 10 shows half of the machine with the stator slots made of steel on top and one row of magnets on the rotor colored in green and red on the bottom. The reduction of the electric machine by one half speeds up the simulation and is possible due to symmetry of the electromagnetic effects. The key features and measurements are summarized in Table 2.

Table 2: Axial Flux Motor Design Parameters

Specification	**Value**
Outer Diameter	280mm
Inner Diameter	180mm
Number of Poles	22
Number of Slots	24
Rotor/Stator Iron Material	M330-35A
Magnet Material	N42
Winding	2 Layer Distributed Copper Winding

The 2D geometry, along with the length of the motor and the material properties allowed for calculating the weight of the electric motor. Table 3 shows the weight estimates for the components of the axial flux machine including an empirical correction factor of 0.82 to account for the weight reduction when transforming from the linear to the AFM configuration.

Table 3: Motor Component Mass Estimates

Motor Component	**Mass [kg]**
Stator	20.8
Rotor	2.1
Magnets	6.2
Windings	4.5
Total	**33.6**

As a main result of the electromagnetic FEA, inductances and the magnetic flux linkage of the motor were used to build an electrical equivalent circuit of the electric motor. This electrical equivalent circuit was integrated into the system model and interacted with the surrounding components such as inverter, battery, and rotor shafts.

A conventional radial flux motor was designed to drive the pusher propeller. Based on the 2D linear motor design shown in Figure 10, a thermal model of the motor was created to investigate the heat propagation and temperature distribution throughout the different motor components during the coupled simulation.

Therefore, a 3D model of the motor was derived from the 2D motor geometry, as shown in Figure 11.

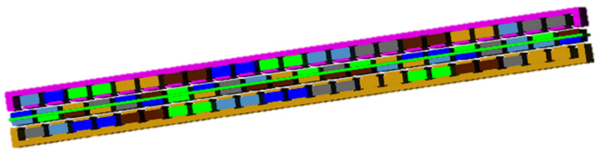

Figure 11: 3D Thermal Motor Model

From the 3D geometry a 1D lumped thermal mass model was derived. The 1D thermal mass model reduced the 3D geometry into a set of point masses, heat sources, and thermal resistivities. Thermal conductivities of materials and contact areas between surrounding parts were derived from the 3D geometry automatically. This 1D reduction allowed for integrating the thermal model into the system model and to investigate the interactions between the thermal motor model and the electromechanical motor model during the runtime of the coupled simulation.

Inverter Design Refinements

The inverter was designed using the browser-based GT-POWERFORGE application. The application allows users to select and compare multiple inverter designs which fit the operating conditions of the electric motor such as AC-power, DC-voltage, and frequency of the 3 phase winding currents. The inverter design tool allows to perform large parametric studies including multiple switch technologies and control strategies to find the optimal power-converter design. The tool also provides estimates for component cost and weight.

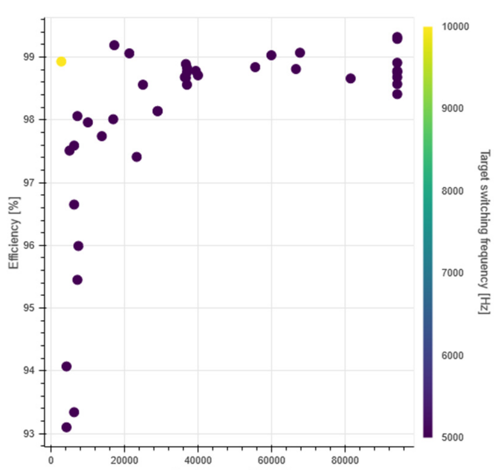

Figure 12: Inverter Efficiency as Function of Specific Power

The inverter efficiency as a function of the specific power from GT-POWERFORGE is shown in Figure 12. The figure shows that the inverter efficiency is low for low specific power inverters. The initial inverter model selected had approximately a mass of 12 kg, a volume of 0.00662m^3, and a global efficiency of 97.5%. Next, the power-loss map of the power-converter was exported to describe the efficiency of the inverter as a function of the electric operating conditions. The exported power-loss map shown in Figure 12 was then integrated into the coupled system model.

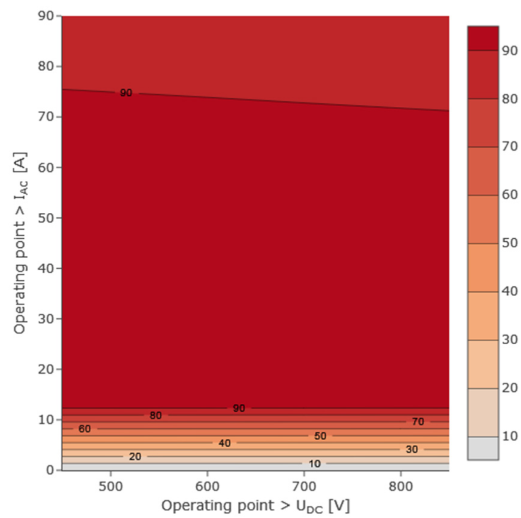

Figure 13: Inverter Power Loss Map

The efficiency and power loss maps were reported as a function of AC-voltage DC-voltage and power factor of the sinusoidal output current of the inverter. While Figure 13 gives the inverter power-loss at one operating point, the complete set of power-loss maps including all dependencies was implemented in the coupled system model.

2.6. Turbulent Airwake Model

Aircraft operations from rooftop vertiports is a key requirement from the business cases and the derived design mission. This demanding operating environment must therefore be considered early in aircraft design for sizing the powertrain components and developing the flight control system requirements. Prior to executing extensive tests and experiments, the authors explored the landing and hover hold simulation within a turbulent airwake for a better understanding of the aircraft design space.

FLIGHTLAB provides a modeling template for including a statistical airwake model at a landing location including a ship deck or building rooftop, see Refs. 8 through 11. A statistical, multi-dimensional full field ship airwake turbulence model was successfully integrated into FLIGHTLAB and validated against the power spectral density of both measured and CFD computed ship airwake data in Ref. 11. The correlations were excellent in the frequency range of the flight dynamics applications. Using the full field ship airwake turbulence model, the multi-dimensional spectral function of the ship airwake was constructed from either CFD or measured data. The spectral function thus obtained naturally reflected the frequency variation of the unsteady airwake over the entire ship domain.

The investigations in Ref. 1 used a scaled ship airwake as a substitute for urban airwake data. For this study, an unsteady simulation for the building depicted in Figure 14 was computed by a Lattice Boltzmann Method (LBM) solver for a 4.5 m/s (15 ft/s) wind emanating perpendicular from the left (Figure 14) of the building. After transients, the volumetric data were interrogated to form a volumetric table look-up with ~0.4m separation distances. This table look-up provides a precursor assessment of a Representative Environment Model (REM) under development under NASA funding for AAM applications, Ref. 13.

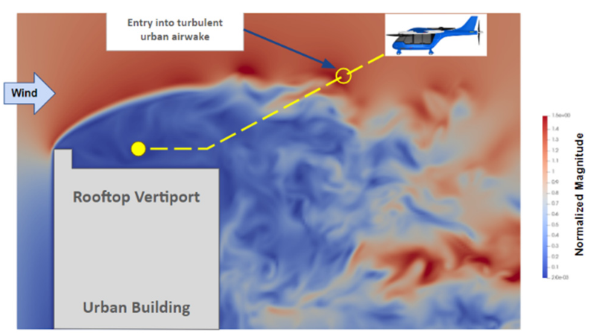

Figure 14: Notional Urban Airwake Structure and eVTOL Landing Zone

2.7. Malfunction Modeling and Simulation

The maneuvering flight simulation for the eVTOL approach into and hover in a turbulent airwake provides transient power requirements as a supplement to the steady state power predictions from the mission performance assessment.

Simulation provides the unique capability to fail aircraft components safely for investigating the effects of faults and malfunctions on the aircraft flight and mission performance. This inherent capability can be exploited during early aircraft design for further refinement of the aircraft and system design requirements.

In this study, the example lift plus cruise eVTOL configuration was simulated to experience a propulsion component failure while operating within the urban airwake. The capability of the flight control system to mitigate the effects of the fault and continue the hover-hold mission task over the landing spot was studied. The insight gained from simulation was expected to inform the design of eVTOL aircraft early in the process where system modifications can be cost effectively accommodated.

A single lift rotor failure was considered for this design study. It provides an additional input into the sizing of the electric motors for the lift rotors and their associated hardware. Since failure modes and recovery strategies are not fully developed at the early design stage, a conservative approach for multirotor configurations was employed for the simulation. The failure simulates a torque limiting due to motor overheating of a single electric motor powering rotor-1, an outboard lift rotor on the wing leading edge (see Figure 2). The fault mitigation approach was to equivalently reduce the power of the mirrored rotor (i.e., on the other side of the wing). Rotor-8 is the equivalent lift rotor on the opposite, outboard, trailing edge wing. Note that rotors-1 and 8 are rotating in opposite directions helping with the torque balance and thus aircraft yaw control during the fault event. Initially, a simple trim in hover was performed with all rotors operating and with one rotor limited to 50% power leading to a 20% increase in steady hover power required for the remaining lift propellers.

An approximately 25 second approach-to-hover trajectory was simulated within the turbulent rooftop airwake as a next step. The turbulent UAM airwake was based on 10 kts steady wind at 0 deg azimuth. Figure 15 presents the time history of rotors 1 and 8 power for the approach maneuver. At time zero and in trimmed forward ascent, fore and aft lift rotors had slightly different power and thrust settings due to the forward flight condition and the aircraft longitudinal C.G. location. The simulation model crosses the roofline in approximately 13 seconds elapsed simulation time. The controller then reduced forward speed to intercept the hover station.

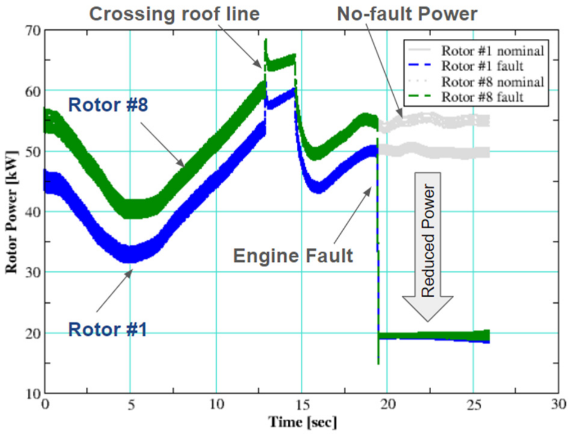

Figure 15: Time History of Rotor Powers in Short Approach and Hover Hold with and without Rotor Failure and in Turbulent Airwake

The rotor-1 failure occurred at approximately 19 seconds with the rotor power dropping sharply 40%, see Figure 15. Rotor-8 power is immediately reduced by the control system to reduce the thrust and torque imbalance. Both lift rotors operate at approx. 20 kW limited power during the fault scenario.

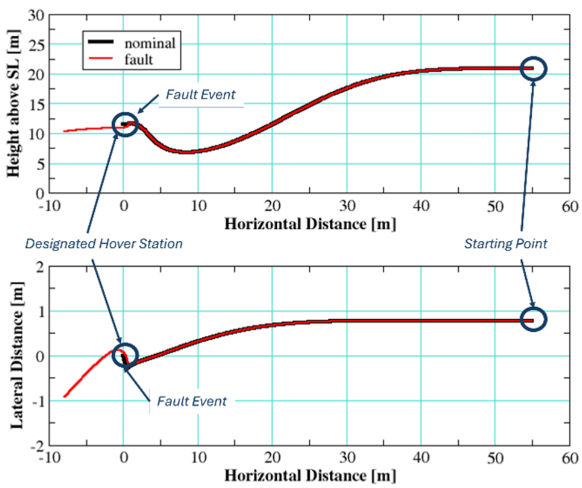

(a) Flight Trajectory

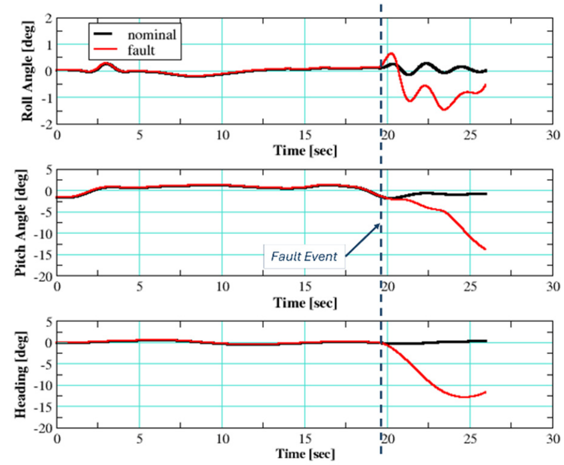

(b) Time Histories of Aircraft Attitudes

Figure 16: Approach Trajectory and Aircraft Attitudes

Figure 16 shows the vertical and horizontal flight trajectories and aircraft attitudes during the approach and hover hold maneuver inside the turbulent airwake. Note that the aircraft was not able to maintain hover position due to the rotor failure and displayed significant divergence in the longitudinal position. This is explained by the change in pitch attitude following the rotor fault. The aircraft pitched nose-down and therefore moved forward. There was also an approximately 15° change in aircraft heading following the fault event. The aircraft roll response was comparatively small. Note that the flight controller was not yet equipped with sophisticated fault response logic.

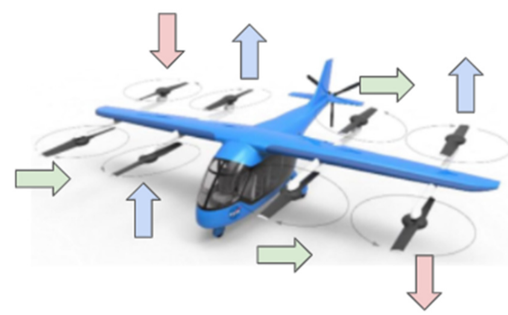

(a) Qualitative Power Change of Lift Rotors

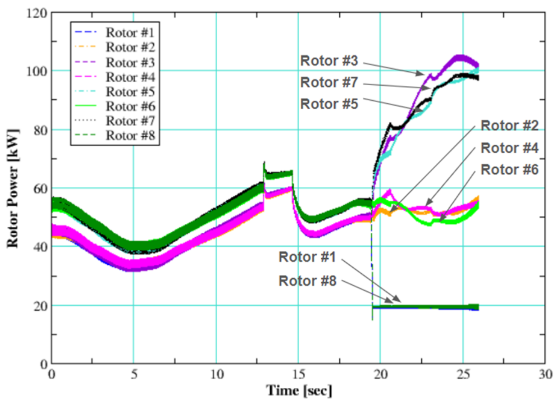

(b) Time Histories of Lift Rotor Power

Figure 17: Lift Rotor Power During Motor Failure and Operations in a Turbulent Airwake

Figure 17 shows the power of all lift rotors as the flight controller attempts to maintain hover position inside the turbulent urban airwake during the fault event. This simulation was performed using the ideal propulsion system in FLIGHTLAB since the coupling with the physics-based electric propulsion system added time delays to the aircraft response exaggerating the inability to maintain hover. Figure 17 shows that three lift rotors did not show any increase in power while three other lift rotors doubled their power demand. This behavior was found to be triggered by the flight control system attempting to maintain heading and pitch attitude. The illustration in Figure 17(a) illustrates the qualitative change in power demand of the individual lift rotors during the fault event. Upwards facing arrows show power increases, downwards decreases, and horizontal facing arrows identify rotors with little power change due to motor failure.

Effect on Motor Temperatures

The results from the motor fault simulation using the ideal engine model (Figure 17b) were executed through the thermal models of the electric motors to analyze the effect of rotor failure on the temperature of motor components.

Figure 18 shows the temperatures of the different motor components with the failure of rotor-1 and power reduction of rotor-8 happening at approximately 20 seconds.

The electric motor failure had the biggest impact on the winding temperature. The time histories of required rotor powers from Figure 17 indicate a high-power demand for rotors 3, 5, and 7 which were reflected in the motor temperatures with winding temperatures of the associated motors rising about 15% over winding temperatures of motors 1 and 8. Magnet temperatures were moderately impacted by the motor power differences while iron temperatures of rotor and stator showed only little impact. This non-uniformity of temperature increase can be explained by the power loss / heat generation behavior of the different motor components.

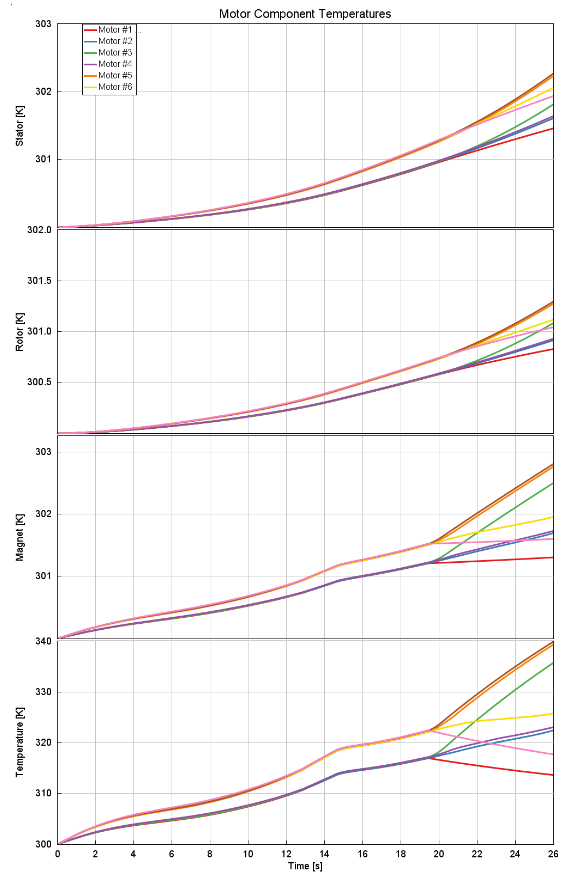

Figure 18: Temperatures of Motor Components During Motor Failure Simulation

The motor speed during rotor failure remained unchanged, while the torque of the electric machine was dropping for failed rotors and increasing for the counteracting rotors. The torque of the electric machine scaled proportional with the imposed current for the implemented motor models. The ohmic heat losses in the copper windings were proportional to the square of the phase current, which was why the winding temperature was sensitive to the power changes of the individual motors. It may therefore be assumed that the thermal fault event of rotor-1 originated in the motor windings.

Conducting the lift rotor fault case in representative operating conditions targeted by the aircraft mission profile, i.e., rooftop landing, provided some important insights for the next design iteration:

- Marginal yaw control of the lift-plus-cruise configuration at low-speed and hover will provide challenges for maintaining aircraft heading during engine failure scenarios.
- Reducing the power equally in the mirrored rotor-8 for a rotor-1 failure, caused difficulties controlling the pitch axis and lead to a significant divergence in longitudinal hover position.
- Three of the remaining, healthy rotors required a 100% increase in power to recover from the fault event which may be considered for sizing the motors, power electronics, and cooling.
- Three lift rotors showed no effect in power demand due to the engine fault. There may be better control strategies that can be developed to recover from a rotor failure.
- Motor winding temperatures of the motors with increased power output increased 15% during the fault simulation.
- The flight control system could fly an approach and hover hold maneuver within the UAM turbulent airwake. However, in the rotor fault scenario, the flight control system shows deficiencies that need to be addressed in the follow-on design iteration.

3. COUPLED FLIGHT DYNAMICS AND ELECTRIC PROPULSION SYSTEM SIMULATION

3.1. Coupled Simulation Environment

The simulation models for flight dynamics and powertrain components described in the previous chapter were combined and connected into a single coupled simulation model. This coupled simulation model was built in GT-SUITE and is illustrated in Figure 19. The motor control value was the rotor speed provided by the FDM. The electric propulsion system provided the motor shaft torques to drive the rotors in the FDM and to maintain constant rotor speeds. The FDM provided the aircraft states for the landing and hover-hold mission task while the powertrain model provided the states of the electric propulsion components.

A runtime model of the FLIGHTLAB FDM was generated as a functional mockup unit (FMU). A functional mock-up unit is a standardized container for simulation models that encapsulates both the model description, and the compiled binary code (runtime model) required for simulation. It follows the Functional Mock-up Interface (FMI) standard, which ensures compatibility across different simulation environments. FMUs can be used integrated in simulation environments that support the FMI standard. FMUs facilitate a flexible and standardized approach to model integration and simulation, enhancing collaboration and efficiency in model-based design and analysis. The FLIGHTLAB FMU was integrated in both MATLAB/Simulink and GT-SUITE simulation environments running on standard Microsoft Windows desktop computers.

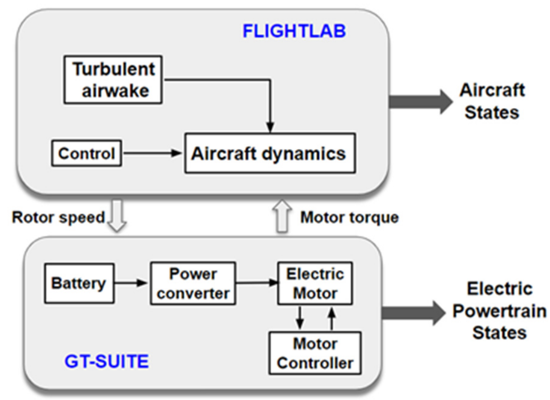

Figure 19: Schematic of FLIGHTLAB and GT-SUITE Coupled Simulation Environment (Ref. 1)

The mechanical model of the electric motor shafts acted as the interface between flight dynamics and powertrain models. While flying a mission, the flight dynamics model calculated a load torque based on propeller speed and blade collective pitch. The rotor load torque was imposed onto the physics-based electric motor, i.e., motor shaft. A motor controller in the propulsion model maintained a constant shaft speed. The motor current was adjusted to compensate for the varying motor torque while maintaining the constant propeller speed during mission task simulation.

The electric motor model received the three-phase current demands from the motor controller. The nine electric motors were controlled individually and were connected to nine individual power converter models. According to the AC current demands the inverters demanded a certain power load from the battery pack, based on the inverter efficiency at the specific operating point. This power demand was imposed on the battery pack and led to a state of charge reduction of the battery pack as the motors pulled current from the battery pack. The torque of the electric motors was passed to the flight dynamics model where it was directly applied to the rotor/propeller shaft.

Consequently, the motor torque included delays in motor controls, limitations of the electrical components and mechanical inertias. This resulted in a full coupling of both simulation models and allowed studying the interactions between flight dynamics and powertrain components in a high degree of detail.

Along with the electric powertrain components described above, thermal models of the electric motor and the battery pack were integrated into the coupled simulation model. Figure 20 shows the final assembly of the coupled simulation model including the flight dynamics FMU, electric powertrain and thermal models in one single simulation model.

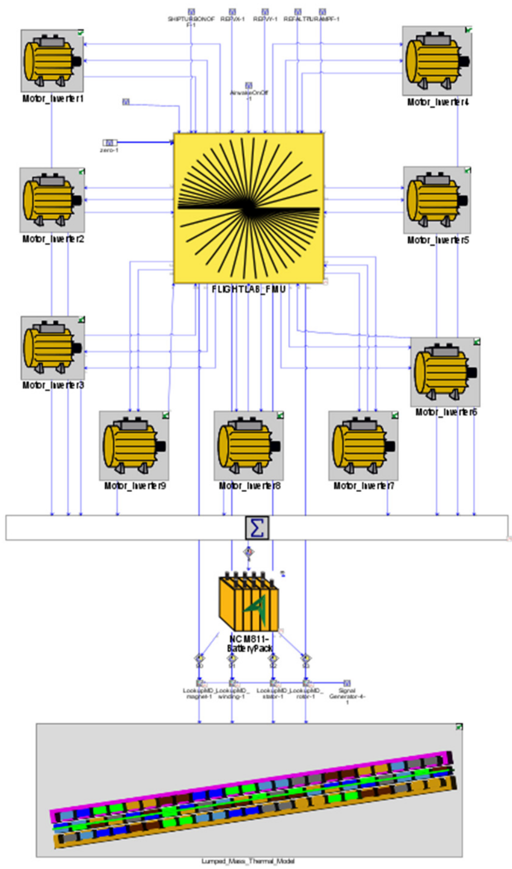

Figure 20: Coupled simulation model in GT-SUITE

The flight dynamics model, the electric powertrain models, and the input/output communication were executed at a constant time step of 0.0018 seconds. Note that the electric powertrain used dynamic time stepping while the maximum timestep was limited to 0.0018 seconds to ensure stability of the coupled simulation.

3.2. Baseline Coupled Simulation Results

A hover hold simulation was performed as a baseline simulation case for the current aircraft design iteration. The mission starts with the flight dynamics model trimmed at a steady, head-on wind of 10 kts in hover with a user-specified height above the landing spot. For the initialization of the electric propulsion system in the coupled simulation and before running the hover-hold mission task element, the flight dynamics body motion was frozen to allow the motor controller to balance the demanded motor torque while maintaining the required constant motor shaft speeds. After propulsion system initialization, the body-motion degrees of freedom in the FDM were unfrozen and the eVTOL model flight trajectory was recorded. Figure 20 shows the displacement in the horizontal (x-y) plane and Euler angles during hover-hold.

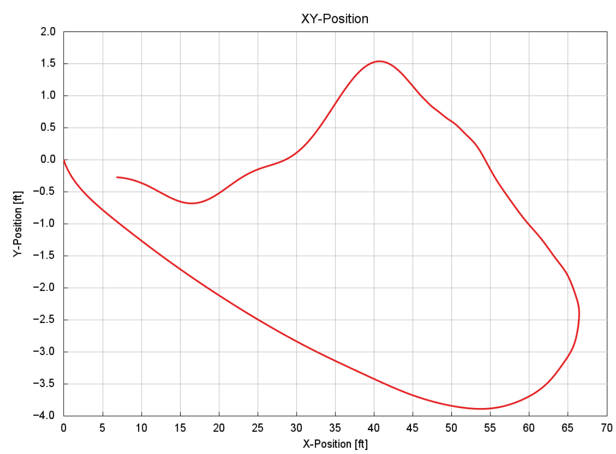

(a) Horizontal Flight Trajectory (x-y)

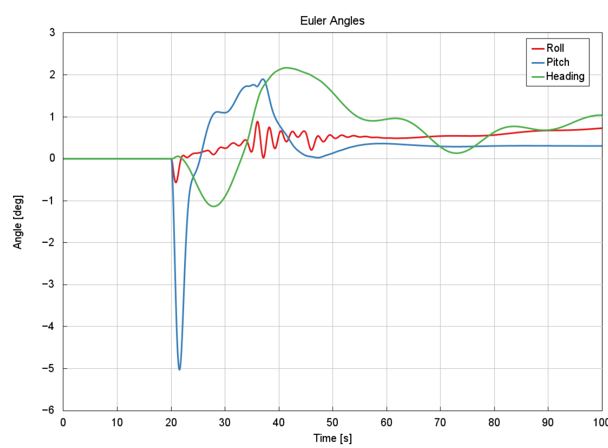

(b) Aircraft Attitudes

Figure 21: Aircraft Horizontal Trajectory and Attitudes during Hover Hold in the Turbulent Airwake

High pitch angle deviations at the beginning of the simulation lead to a high displacement in longitudinal direction while the lateral displacement remains comparably small. After initial deviations from the hover position for all the Euler angles, the flight control system stabilized the model within a few seconds and the model returned to the desired hover position.

The angular displacements of the eVTOL can also be investigated from the torque produced by the motors. Figure 22 shows a comparison of motor torques of motor-1 and motor-5 according to the results shown in Figure 17.

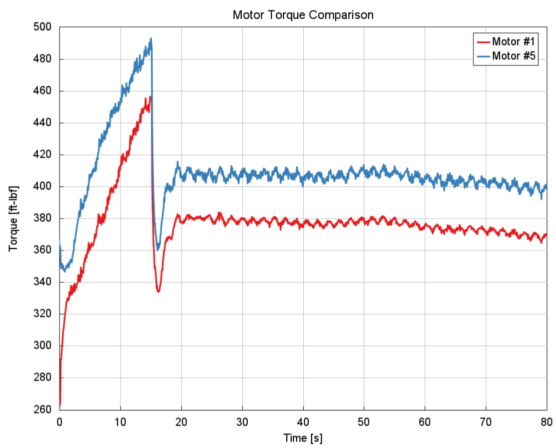

Figure 22: Motor Torque Comparison

The first 20 seconds of the coupled simulation were used for initialization of the propulsion model to ensure that the motor controls stabilized before releasing the body degrees of freedom of the coupled simulation in hover hold. In Figure 22, both motors ran at the same rotational speed. Motor-5 produced more torque than -1 due to a difference in collective blade pitch settings from the flight control system. Consequently in Figure 21, the initial pitch attitude excursion after 20 seconds (model release) resulted from a difference in forward/aft lift rotor thrust.

While the motors were running, power losses in the form of heat were imposed onto the different motor components. The electromagnetic FEA allowed to calculate motor losses for rotor, stator, magnets, and windings inside the motor. These losses were dependent on the speed and torque of the electric motor and were imposed onto the thermal mass network of the electric motor. This allowed for analyzing the heat propagation and temperature distribution inside the motor models. Figure 23 shows the temperatures of the different motor components throughout the hover-hold mission element simulation.

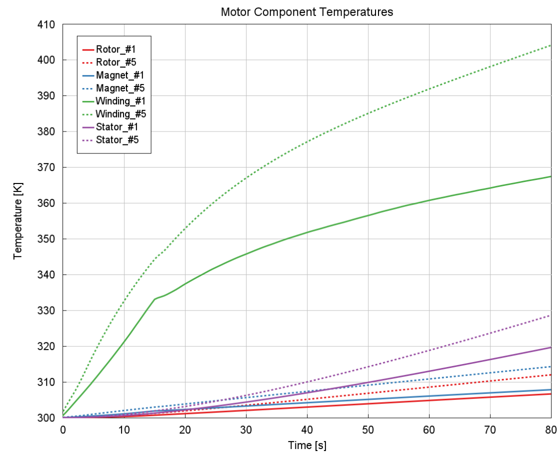

Figure 23: Temperatures of Motor Components during the Hover Hold Mission Element

The data was plotted for both motor-1 and motor-5 in Figure 23. Magnet and rotor temperatures showed a moderate increase of less than 10 Kelvin over the course of the hover hold. The main heat source in the motor was the copper windings. Especially in operating conditions characterized by high motor torque and low motor speed, the copper losses were expected to be the dominating source of heat inside a motor. This high heat production inside the windings heats up the stator iron material, which can be seen in Figure 23. Consequently, as motor-5 produced more torque during the hover-hold mission element, the ohmic losses inside the motor windings increased and the temperatures inside the motor windings rose.

4. TASKS FOR THE NEXT DESIGN ITERATION

The design iteration exercised in this study provided important insights and requirements for the design of the flight and propulsion systems. The system weight estimates using the GT-SUITE sizing tools in this design iteration are summarized in the bill of materials in Table 4. Note that the insights gained from the initial heat management models in this iteration will enable the required refinement of the electric propulsion components and thus yield component mass estimates for the thermal system in the next design iteration.

Table 4: Propulsion System Bill of Materials

Component	QTY	Mass
e-Motor (lifter)	8	33.6 kg
e-Motor (pusher)	1	41 kg
Inverter	9	12 kg
Battery Pack	1	859 kg
Heat Management	-	TBD
Total		**1,276.8 kg**

The findings of this design iteration and tasks for the next iteration can be summarized as follows:

- Update aircraft weight and balance with information from this iteration, re-calculate useful load margins, and rerun mission performance simulation if needed.
- Optimize the powertrain components based on system performance. This includes optimizing motor and inverter design based on targeted traveling range of the eVTOL or steadiness of flight in turbulent airwake.
- Investigation of different cooling concepts for the electric powertrain components, e.g. spray-cooling, oil-cooling or different cooling pipe layouts. This will also provide an initial mass estimate for the cooling components.
- Implement the pusher propeller in low-speed control laws and fault detection and mitigation logic.
- Tune flight control gains to improve operations of the coupled simulation in the turbulent airwake environment and to more tightly maintain the approach trajectory and hover position.
- Improve yaw control in hover and low speed.
- Optimize battery sizing and recharging strategy for potential system weight reduction.
- Advance single-motor failure detection and mitigation strategies in the propulsion and flight control systems. Flight control improvements will aim to avoid excessive power drawn from the remaining, healthy electric motors.
- Expand flight dynamics model to include starting/stopping of lift rotors in preparation of flight transition simulation between VTOL and fixed-wing modes.
- Perform a parametric study of approach and hover-hold simulations with the coupled system and for additional wind velocities, wind directions, and turbulence strength conditions.

5. SUMMARY AND CONCLUSIONS

A single conceptual aircraft design iteration was performed in this study exploring the application of detailed flight dynamics and electric propulsion simulation to derive aircraft and system requirements for a notional lift plus cruise eVTOL configuration. An initial flight dynamics model was used to estimate the aircraft design mission performance for sizing the main components of the electric propulsion system. To expand the detail of information for component sizing and to derive requirements for the propulsion and flight control systems by adding the maneuvering power demand, a landing approach trajectory into an urban airwake was modeled.

The simulation of a single motor failure during a hover-hold mission element within the turbulent urban airwake provided initial insights into the emergency power required from the remaining, healthy lift rotors. This information was used to refine the requirements of the propulsion system as it impacted battery power draw and heat generation.

A coupled simulation of flight dynamics and detailed electric propulsion system was performed for hover-hold in the urban turbulent airwake imposing realistic time constants to the flight control system and this exposing required improvements of the flight and propulsion control logics. The detailed propulsion system model provided the required insight for developing cooling strategies for the propulsion components.

The detailed early simulation also provides initial mass estimates for key power components important for the aircraft design. The insights from using detailed and coupled aircraft simulation in this aircraft design iteration were summarized as a task list for the follow-on aircraft design iteration. The study thus demonstrated the effective application of coupled aircraft simulation early on in aircraft design for developing important requirements for the aircraft system design, specifically for the flight control electric propulsion systems and particularly for operations in the urban environment.

ACKNOWLEDGEMENT

Authors would like to thank Dr. Marilyn J. Smith and her team at the Georgia Institute of Technology for providing the representative urban turbulent airwake predictions for this study.

6. REFERENCES

1. Goericke, J., Brenner, F., Lee, Dooyong, Habana, Zoren, “Investigation of eVTOL Operations in Turbulent Airwake using Comprehensive Rotorcraft Analysis and Physics-Based Electric Propulsion System Models,” VFS 6th Decennial Aeromechanics Specialists’ Conference, Santa Clara, CA, USA Feb.6-8, 2024

2. Brenner, F., Goericke, J., Hasbun, M., “Comprehensive Simulation for eVTOL Aircraft-Diagnosing Coupled Airframe-Propulsion Dynamic Instabilities,” 78th Vertical Flight Society Annual Forum, Ft. Worth, TX May 2022

3. Brenner, F., Goericke, J., Hasbun, M., “Comprehensive Simulation with Coupled Airframe-Propulsion Dynamics in Support of eVTOL Design,” 79th Vertical Flight Society Annual Forum, West Palm Beach, FL May 2023

4. Hoff van’t, S.; Lu, L.; Padfield, G.; Podzus, P.; White, M.; Quaranta, G.; “Preliminary Guidelines for a Requirements-Based Approach to Certification by Simulation for Rotorcraft,” 48th European Rotorcraft Forum, Winterthur, Switzerland, 6-8 September 2022

5. Simmons, B. M., Bunning, P. G., and Murphy, P. C., “Full-Envelope Aero-Propulsive Model Identification for Lift+Cruise Aircraft Using Computational Experiments,” https://www.researchgate.net/publication/353539418, August 2021

6. Silva, C. and Johnson, W., “VTOL Urban Air Mobility Concept Vehicles for Technology Development”, 2018 Aviation Technology, Integration, and Operations Conference, AIAA Paper 2018-3847, June 2018, https://doi.org/10.2514/6.2018-3847

7. Mahmoudi A., Rahim N. A. and Hew W. P., “Axial-flux permanent-magnet machine modeling, design, simulation and analysis”, Scientific Research and Essays Vol. 6(12), pp. 2525-2549, 18 June 2011

8. He, C., Lee, D., Zhao, J., Ware, C., “Unified Control and Simulation Tool in Support of Rotorcraft/Ship Dynamic Interface," AHS 67th Annual Forum, May 2011

9. Xin, H. and He, C., ``A Statistical Turbulence Model for Shipboard Rotorcraft Simulations," Proceedings of 63rd Annual AHS Forum, Virginia Beach, VA, May 2007

10. He, C., Kang H., Carico, D. and Long, K., “Development of a Modeling and Simulation Tool for Rotorcraft/Ship Dynamic Interface Testing", Proceedings of 58th AHS Annual Forum, June 11-13, 2002, Montreal, Canada

11. He, C., Goericke, J., Lee, D., and Zhao, J., ``Simulation Development in Support of Investigation of Handling Qualities Specification Requirements for Maritime Rotorcraft," American Helicopter Society Specialists' Conference on Aeromechanics, San Francisco, CA, 23-25 January 2008

12. Polsky, S. A. and Bruner, C. W. S., ``Time-Accurate Computational Simulation of an LHA Ship Airwake," AIAA-2000-4126, 18th AIAA Applied Aerodynamics Conference, Denver, CO, Aug. 2000

13. Smith, M. J., Crawford, A., and Carozza, K., “Development of an Operational Analysis Tool for Urban Air Mobility,” Proceedings of the 79th Vertical Flight Society Annual Forum, West Palm Beach, FL, May 16--18, 2023, 10.4050/F-0079-2023-18135